Batteries & Supercaps

Research Article
doi.org/10.1002/batt.202400006

Chemistry Europe
European Chemical Societies Publishing

www.batteries-supercaps.org

Setup Design and Data Evaluation for DEMS in Sodium Ion Batteries, Demonstrated on a Mn-Rich Cathode Material

Jonas Geisler,*[a] Lukas Pfeiffer,[b] Guillermo A. Ferrero,[a] Peter Axmann,[b] and Philipp Adelhelm*[a, c]

Differential electrochemical mass spectrometry (DEMS) is a powerful operando method for analyzing side reactions in batteries. We describe our DEMS setup highlighting the relevance for implementing a reference electrode. Although the method provides valuable information, the correct assignment of the DEMS signals to types of gases and quantifying the amounts released can be challenging. A frequent limitation is that gas concentrations are calculated from single m/z ratios. This has the drawback of overlooking unexpected gases which can cause misinterpretation of the signal intensities, or even attributing to gases which are not actually formed. We present a multiple concentration determination (MCD) algorithm that uses the full MS-spectra, which allows a more reliable determination of the gas release. We demonstrate this approach for Na-ion half-cells with P2-$Na_{0.67}Mn_{3/4}Ni_{1/4}O_2$ (NaMNO) as cathode active material (CAM). Studying the gassing behavior for two electrolyte formulations (1 M $NaPF_6$ in propylene carbonate (PC) and in diglyme (2G)). Against the general belief that glymes lead to more gassing at high potentials, we find that gas evolution for PC electrolytes is larger compared to 2G electrolytes. Dimethyl ether is found to be a decomposition product of 2G. Pressure change measurements are used to independently validate the gas quantification.

1. Introduction

Sodium-ion batteries (SIBs) are a promising alternative to state-of-the-art lithium-ion batteries (LIBs). They are particularly beneficial as low-cost alternatives that use more abundant resources, which can be obtained from less critical economic, social, and environmental sources.[1–5] The energy density of SIBs can be significantly higher than that of lead-acid or nickel metal hydride batteries, while being close to or even on par with some LIB cell chemistries.[2] Moreover, SIBs can be manufactured using LIB production lines, which implies that the production processes are already available at an industrial scale.[6] However, further research is required to develop materials for SIBs in order to attain a competitive level. This remains the most pressing topic for SIBs to achieve sufficient cycle life.

To enhance battery performance, it is crucial to comprehend gas formation during cell cycling. Gas formation in both LIBs and SIBs usually takes place during cell formation (SEI formation), which releases larger quantities of gases such as CO, CO_2 or C_2H_2.[4,7] Gas may also be released during battery cycling. Gas formation typically indicates undesired side reactions, which may be caused by overcharging or overdischarging. These reactions can lead to the decomposition of the electrolyte and/or the electrode materials. Even a very minor gas release can be a sign of continuous cell degradation which limits cycle life. To improve battery performance, it is highly desirable to detect gases and link their formation to parameters such as the state of charge or temperature.[3,4,7] Differential electrochemical mass spectrometry (DEMS) is a method that combines electrochemical measurements with gas analysis.[7–9] It provides information on the types and amounts of gases released during electrochemical experiments. This information can enable a more knowledge-based improvement in materials development and battery cycling conditions.

The properties of Ni–Mn based compounds are currently intensively studied and depend a lot on their exact compositions.[35–37] For example, elements such as Li, Ca, Mg, or Sc are used as substitutional elements for this.[38–41] Gas release can occur due to electrolyte oxidation and/or structural degradation of the positive electrode.[7] Determining the onset potential for gas release when charging the electrode of LIBs or SIBs is a crucial aspect of using DEMS. This is especially relevant for SIBs, as the layered oxides show a very sloping voltage profile,[5,10] which makes it difficult to determine an upper cut-off potential that allows for safe and prolonged cycling. Most of the layered oxides studied for SIBs are cycled above 4 V, which can cause electrolyte decomposition. To determine the relevant

[a] J. Geisler, G. A. Ferrero, P. Adelhelm
Institut für Chemie, Humboldt-Universität zu Berlin, Brook-Taylor-Str. 2, 12489 Berlin, Germany
E-mail: jonas.geisler@hu-berlin.de
philipp.adelhelm@hu-berlin.de

[b] L. Pfeiffer, P. Axmann
Accumulators Material Research (ECM), ZSW Center for Solar Energy and Hydrogen Research Baden-Württemberg, 89081 Ulm, Germany

[c] P. Adelhelm
Joint research group Operando Battery Analysis (CE-GOBA), Helmholtz-Zentrum Berlin, Hahn-Meitner-Platz 1, 14109 Berlin, Germany

Supporting information for this article is available on the WWW under https://doi.org/10.1002/batt.202400006

electrode potentials precisely, it is generally advantageous to use a 3-electrode setup.

Only a few DEMS studies on SIBs have been published to date, most of them in the last years.[11–19] While there is more knowledge on gassing in LIBs,[4,7,20,21] not all of it can be easily applied to SIBs. In half-cell configurations, Li or Na are commonly used as a counter electrode. However, the higher reactivity of Na metal and the increased solubility of degradation products in the electrolyte solvents lead to new challenges.[11] Also, the storage mechanism, as in the case of graphite, may be entirely different.[5]

Most publications focus on cells with carbonate-based electrolytes as they are the most common electrolytes in LIBs.[11,14–16,18] Much less is known about the stability of ethers although they are attractive solvents for next generation batteries.[22] A popular ether solvent is diglyme (2G). Due to its favorable stability at low (reductive) potentials, it has been utilized to study a variety of anode materials, such as Sn[23–25] or graphite,[12] as well as various types of full-cells with Na metal as an anode.[26,27] On anode materials, 2G is believed to form a thin and stable SEI through ether polymerization.[13,24,28] Possible decomposition products may include ethane, methane, and dimethyl ether; however, they are not always detected. For example, Tsiouvaras and Meini *et al.* confirmed the formation of dimethyl ether in Li-O_2 batteries,[29,30] while Qin *et al.*, found only H_2 release on the tin anodes in SIBs.[13] It is generally believed that ethers are less stable at high (oxidative) potentials.[31] The evolution of gas in SIBs can be significantly influenced by the conductive salt. This has been demonstrated in various 2G electrolyte formulations for graphite electrodes or symmetric Na|Na cells.[17] However, there is limited information available on the gassing behavior of SIBs overall.

The publication is divided into two parts. The first part describes the DEMS setup and data processing using a multiple concentration determination (MCD) algorithm. The second part, discusses the results of the DEMS analysis for sodium manganese nickel oxide ($Na_xMn_{3/4}Ni_{1/4}O_2$, abbreviated as NaMNO) as the working electrode[32–34] and Na metal as the counter electrode. The gas formation was compared for two different electrolyte formulations using 2G and PC as solvents, with $NaPF_6$ as the conductive salt, and for two different upper cut-off potentials. When exceeding redox potentials of 3.8 V vs Na^+/Na, CO_2, methane, and dimethyl ether were found as decomposition products in case of 2G.

2. Method

2.1. Technical Aspects of the DEMS Setup

Before discussing the method, it is important to note that there is no consistent terminology for determining gas release during electrochemical experiments using mass spectrometry. The term *'online* electrochemical mass spectrometry' (OEMS) refers to the measurement system where the MS is applied *online* to the cell,[42,43] which is applicable to the system described here. At the same time, the measured signals represent the *differential* to the accumulated gases over time. The system presented here has a high enough time resolution to generate *differential* signals in reference to the time scale of the cell cycling. This is achieved by using a carrier gas, that purges the formed gases from the cell.[44,45] For these systems, the term *differential* electrochemical mass spectrometry (DEMS) was coined.[8] This method differs from others that have similar time resolution but measure accumulated gas amounts over time.[43,46,47] Although, both terms generally apply to the method discussed here, we will use only the term DEMS for simplicity.

The cell design is based on the setup developed by Berkes *et al.*,[45] but it has been extended by implementing a sodium metal reference electrode. This allows for monitoring the electrode potentials of both the working and counter electrodes, which is crucial determining the maximum possible cut-off potential of the layered oxide with precision. This is particularly relevant in full-cell experiments, which will be part of a forthcoming study. Even in half-cells, the use of a reference electrode can be important as the polarization of the counter electrode may strongly depend on the electrolyte formulation. This can drastically influence the cut-off potential reached at the working electrode. Although there is a clear benefit when measuring in three-electrode geometry, there are known limitations of sodium metal as a reference due to its reactivity towards electrolytes. Na–Sn has been proposed as an alternative reference electrode.[48] However, caution must be exercised due to the complexity of the phase diagram. Additionally, the presence of other components, such as tin, in the DEMS measurement may affect the overall behavior of the cell. This could potentially compromise the comparability of the results, particularly for gas-forming side reactions. On the other hand, several publications demonstrate the extended and stable cycle life of electrode materials in half-cells with Na metal as a counter electrode. Therefore, a relevant potential drift in our experiments is unlikely. The cells underwent a 24 h equilibration period. The voltage plateaus of the cathode materials (Figure 6 and Figure 7) being at the same potentials suggest that any difference in the potential of the reference in the different solvents should be negligible.

The measurement cell as illustrated in Figure 1A) was designed to be comparable to other commonly used research cells such as Swagelok® type cells or coin cells.[49] The distance between the working and counter electrodes was also reduced to minimize the electrolyte volume, a common limitation of many DEMS cells..[42,50–52] However, a drawback of commonly used coin or Swagelok-type cells is the small electrode size, which is typically around 1 cm^2. To improve the MS signal-to-noise ratio in this study, we used larger working electrodes (11.24 cm^2) because smaller electrodes produce less gas and make it more difficult to reach the detection limit of the MS. For other instruments, electrodes cast on porous membranes are used.[42,51,52] We opted for electrodes cast on standard current collectors, specifically aluminum foil, to ensure comparability with other experiments.

The current collector for the working electrode is structured with a gas flow field. To enhance gas diffusion from the electrolyte into the carrier gas stream, the working electrode

Research Article
doi.org/10.1002/batt.202400006
Chemistry Europe
European Chemical Societies Publishing

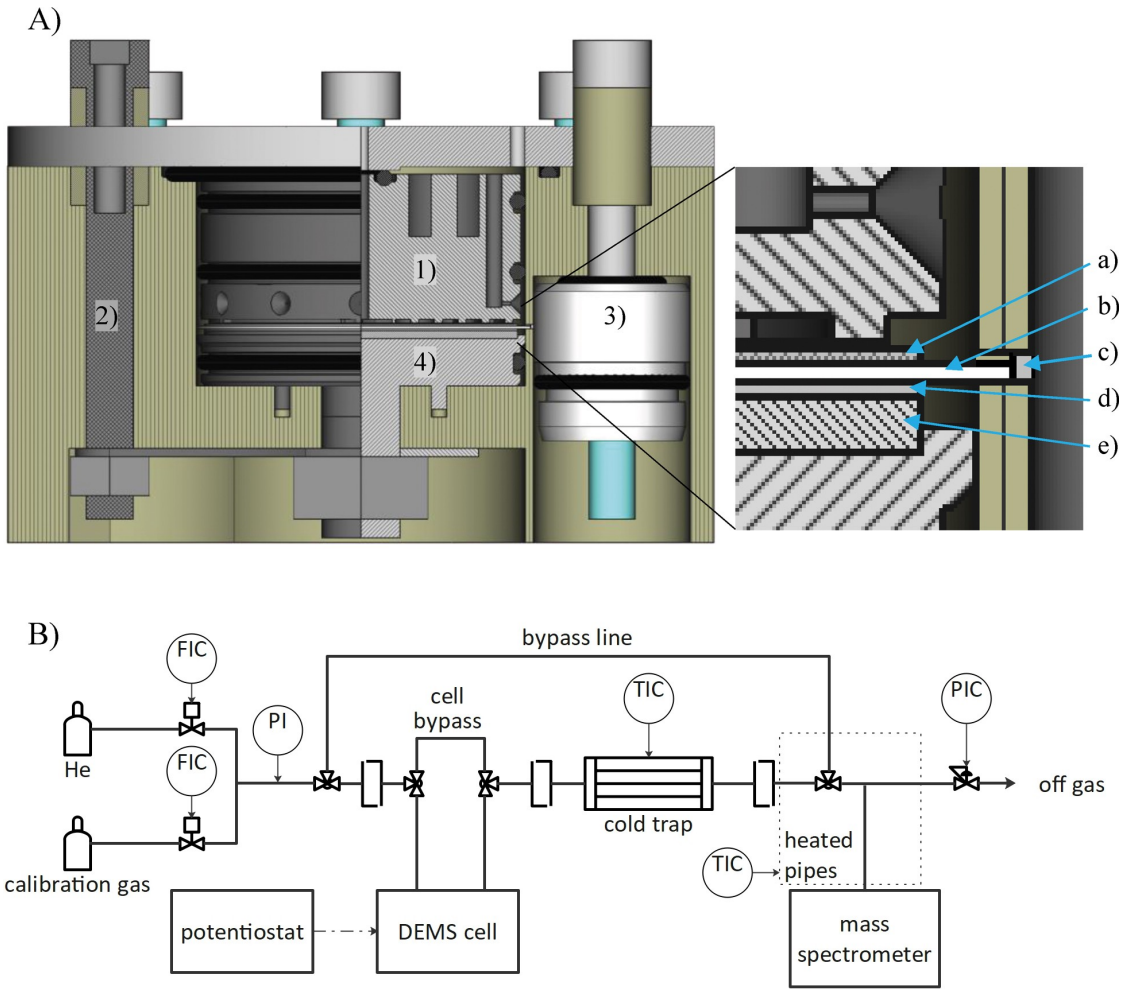

Figure 1. A) DEMS cell design, for three electrode measurements.1) working electrode current collector with gas flow field; 2) connection to counter electrode current collector from top of the cell; 3) reference electrode current collector; 4) counter electrode current collector; a) working electrode on current collector foil; b) separator; c) reference electrode (sodium metal); d) counter electrode (sodium metal); e) counter electrode mounting plate.
B) Process flow diagram of the DEMS measurement setup. Legend of letter symbols for measurement and control units: C = controller, F = flow, I = indicator, P = pressure, T = temperature.

current collector foil has been perforated with a needle roller. Figure 1 B) provides a flow diagram of the overall system. Helium is used as a carrier gas with a flow rate of 5 NmL h^{-1}. Helium is preferred as a carrier-gas because it exerts less sputtering stress on the internals of the MS compared to argon. The system is supplied with helium via a mass flow controller. The second mass flow controller is an inlet for calibration gas mixtures. This enables calibration of the system with adjustable molar fractions of calibration gases by further diluting the calibration gas mixture with pure helium. The connections and valves are made from stainless-steel Swagelock® parts.

To reduce the background signals from electrolyte solvent molecules, a cold trap (−30 °C) is added after the cell. A PTFE screw cap system rated for vacuum applications is used to connect the stainless-steel tubing to the cold trap, which uses a glass tube. The cold trap condenses majority of the evaporated solvent, resulting in improved background. It is crucial to minimize high signals from the solvent background to reduce noise and facilitate accurate data assignment to specific gases. This is a problem with other types of setups.[42]

Behind the cold trap, the gas stream is continuously sampled through the inlet capillary of the MS, a Pfeiffer Vacuum OMNISTAR™ GSD320 with a range of 1–200 Da. The system is maintained at a pressure of 1.6 bar to prevent diffusion of air traces into the system. To ensure a constant pressure and hence constant sample gas flow into the MS, a back-pressure regulator is used after the junction to the MS. The residual gas is vented to the exhaust system.

A sudden change in gas concentration can be detected after a response time of approximately 30 s, resulting in a peak width of around 5 min. Compared to electrochemical processes, which take about 10 h per half cycle, the signal response is quasi instantaneous.

The system enables measurements exceeding 200 hours, allowing for the study of multiple charge/discharge cycles. Such measurement times are significantly longer than the 10–

30 hours those reported for other systems.[29,53] Exceeding 200 hours can result in erratic results due to the cell drying out.

2.2. Data Processing

General approach: Another focus of this work was to improve the processing of data from DEMS measurements in battery research. The conventional method of analyzing DEMS data involves quantifying a specific gas using one m/z ratio.[11,13,16,17,42,45,53–58] However, overlapping signals from different gases can lead to misinterpretation. To address this issue, signals are often corrected for contributions from other gases with known concentration.[58,59] Alternatively, a less precise method is to define a m/z signal to a specific gas without correction.[11,16,17,54–56] Both methods require an educated guess by the researcher, but overlapping signals can make it challenging to identify and quantify gases, particularly when unexpected or unknown gases are formed. For instance, a mass of m/z = 28 can correspond to CO, N_2 or C_2H_2, for example. This demonstartes that identifying a specific gas and determining its quantity can be difficult, particularly when unknown gases are also present.

In this work, we take a different approach by analyzing the full mass spectra between 1 to 100 m/z instead of detecting single m/z values. The most probable concentrations are fitted using a multiple concentration determination (MCD) algorithm based on the intensities of all m/z ratios. Therefore, an additive overlap of the individual spectra of the expected species is calculated, using the least-squares method to fit this to the baseline corrected spectra. This analysis provides quantitative gas evolution rates for all expected gases from the full spectra, using a suitable calibration. The approach described has been applied to mass spectrometry in the past[60] but, to the best of our knowledge, has never been applied to DEMS studies of Li-ion/Na-ion batteries. He and Lundström *et al.* used a similar mathematical approach for DEMS in batteries, but only using selected m/z values for expected gases.[61,62] In this case, unexpected gases might be overseen. The contributions of unexpected gases to the signals of expected gases can lead to misinterpretation. The described protocol, allows for verification of the results and identification of any unexpected gases. A detailed example is provided in the supporting information.

The DEMS measurement's raw data undergoes pre-treatment, including smoothening, normalization, and baseline correction, before calculating gas concentrations. Figure 2a)–c) compares the data from raw data through the different steps of pretreatment. Note that m/z values of 1, 3 and 4 were excluded for the analysis. For a more detailed description of the algorithm, please refer to the supporting information.

The initial step, involves smoothing the raw data. Gas concentration may vary during acquisition of a single spectrum. This is due to the difference between the system's response time (approximately 30 s) and the time required to acquire the full spectrum (approximately 100 s). To address this issue a Gaussian smoothing is applied over five spectra. The smoothing process was found to maintain signal sharpness without blurring or broadening, while also smoothing out concentration changes over a few spectra. The impact of signal smoothing on

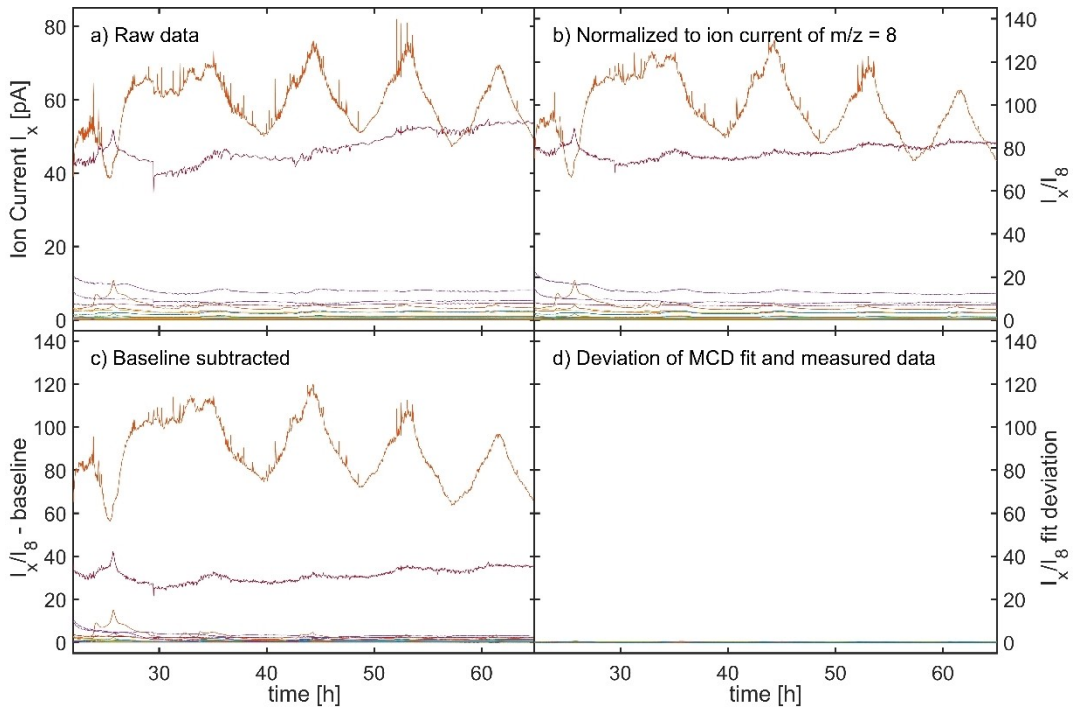

Figure 2. Steps of the data processing for the example of a NaMNO cell with 1 M $NaPF_6$ in PC as electrolyte with sodium metal counter and reference electrodes. a) Raw data of the ion currents Ix for all m/z values evaluated. b) Smoothened signals normalized to Ion current I8 of m/z 8. c) Signals after baseline subtraction. d) Deviation of the signal from norm residual resolution fit to calculate gas concentrations.

the data is demonstrated in the Figure SI-4 Supporting Information.

In the second step, the signals are then normalized to the ion current I_8 of m/z = 8, which is representsonly the Helium dimer ion He_2^+ from the carrier gas. He_2^+ acts as an internal standard in our measurements to correct for the general drift in sensitivity of the instrument over time. Figure 2a) shows the original data measured with the MS for a typical measurement, Figure 2b) shows the smoothed and normalized signals. Finally, the data is baseline corrected. This is done by subtracting the signals from the cell bypass (pure He carrier gas) from the overall signals, as shown in Figure 2c).

The pretreated data is then used for quantifying the different gases. For each single spectrum, the least-square solution is calculated against a calibration table to determine the most probable composition at a given time. This approach assumes that the fragments of the different components do not influence each other, meaning that the measured spectra is the sum of all individual components.

The calibration table was determined using calibration gas mixtures containing He and a set of individual gases in the expected range of concentrations. For each cell, the common decomposition products including H_2, CO_2, and CO, as well as the background gases N_2, O_2, Ar, and water vapor were considered. The sources for the background gases include the cell assembly in the Ar glovebox or residual air and moisture in the tubes and fittings.

The mass spectra of liquids were obtained by filling the cold trap with each individual liquid and changing the temperature of the cold trap. Gas streams with varying concentrations were obtained using this method, and the corresponding spectra were determined. These reference measurements provided qualitative information regarding the contribution of the solvents to the mass spectra during cell cycling. CH_4, dimethyl ether and 2G vapor were measured for cells with 2G-based electrolytes, and propene and PC vapor were measured for cells with PC-based electrolytes. The selection of those gases gave good results. Ethane, ethene and propane were also considered but excluded from the calculation as they were not found in the spectra.

Overall, this approach has a major advantage that it allows for monitoring the entire battery cycling process to determine whether the algorithm provides meaningful results for the entire spectrum (m/z from 1 to 100). This minimizes the risk of missing unexpected gases or incorrectly attributing signals. The quality of the fit was tested by calculating the theoretical spectrum of the measured gas amounts and subtracting it from the original baseline-corrected spectra. In an ideal scenario, the algorithm should attribute all signals in the spectrum to a certain gas concentration, resulting in a zero deviation. However, deviations from this scenario lead to some noise, which may be caused by non-linearities or deviations of the spectrum from the calibration spectrum. Figure 2d) provides an example of such a quality check, which shows a very small deviation, indicating that the approach can deliver reliable results. More detailed information can be found in the supporting information.

2.3. Method Validation Using a Pressure Cell

The DEMS data processing provides quantitative results on the types and amounts of gases released. To validate these results, pressure monitoring during galvanostatic cycling (PMGC),[63,64] can be used as an independent method. PMGC measures the pressure change in a closed cell of defined volume during battery charge/discharge. The pressure change is directly related to the formation of gas, the total amount of gas released can be calculated using the the pressure change, the dead volume of the cell, and the ideal gas law. A commercial device with a two-electrode geometry was used for this purpose. Figure 3 shows a comparison of the accumulated gases measured independently with DEMS and PMGC over the first two cycles of a cell.

The total gas amounts found in both experiments are comparable reaching values of around 200–250 μmol/g. This indicates accurate calibration of the DEMS data and correct assignment of the evolved gases. It is worth noting that the PMGC data also shows an undulating behavior, which is initially unexpected as a continuous release of gas should result in a continuous increase in pressure. However, since the pressure cell is a closed system, some gases may be consumed by successive reactions or diffuse out of the cell over time. The latter would be particularly likely for H_2. The major influence on can be attributed to changes in the volume of the electrodes depending on the state-of-charge. The expansion and shrinkage of the Na metal anode, due to plating and stripping, especially contributes to the observed shape. Overall, the PMGC measurements provide strong support for the analysis of the DEMS data obtained for the cell with the 2G electrolyte.

The PMGC measurements revealed an important aspect regarding the gassing behavior of electrochemical cells. This concerns possible misinterpretation of data when using two- instead of three electrode cells. This aspect can be seen for cells with PC-based electrodes with Na metal as the counter electrode, see supporting information Figure SI-5 and Figure SI-6). Experiments are often conducted in half-cells with Na (or Li) as the counter electrode, providing only the voltage of the cell instead of the individual potential of the working electrode. However, the measured voltage between the working and counter electrode is often incorrectly stated as the electrode potential of the working electrode, i. e. V vs. Na^+/Na. This effect is negligible if the polarization of the Na counter electrode is small, which is the case for the diglyme-based electrolyte (at reasonable currents). For carbonate electrolytes, however, the polarization can be much larger due to a more resistive SEI.[17] The consequence of this is that the upper cut-off potential of the working electrode is effectively reached already at a lower value. For instance, a targeted cut-off potential of 4.2 V vs. Na^+/Na would be effectively reached already at 4.1 V vs. Na^+/Na, if the counter electrode causes a 0.1 V polarization. This is the order of magnitude of the observed polarization for the PC electrolyte, as can be seen in the inset of Figure 4. This indicates, that the stability of the electrolyte may be over-estimated.

Research Article
doi.org/10.1002/batt.202400006
Chemistry Europe
European Chemical Societies Publishing

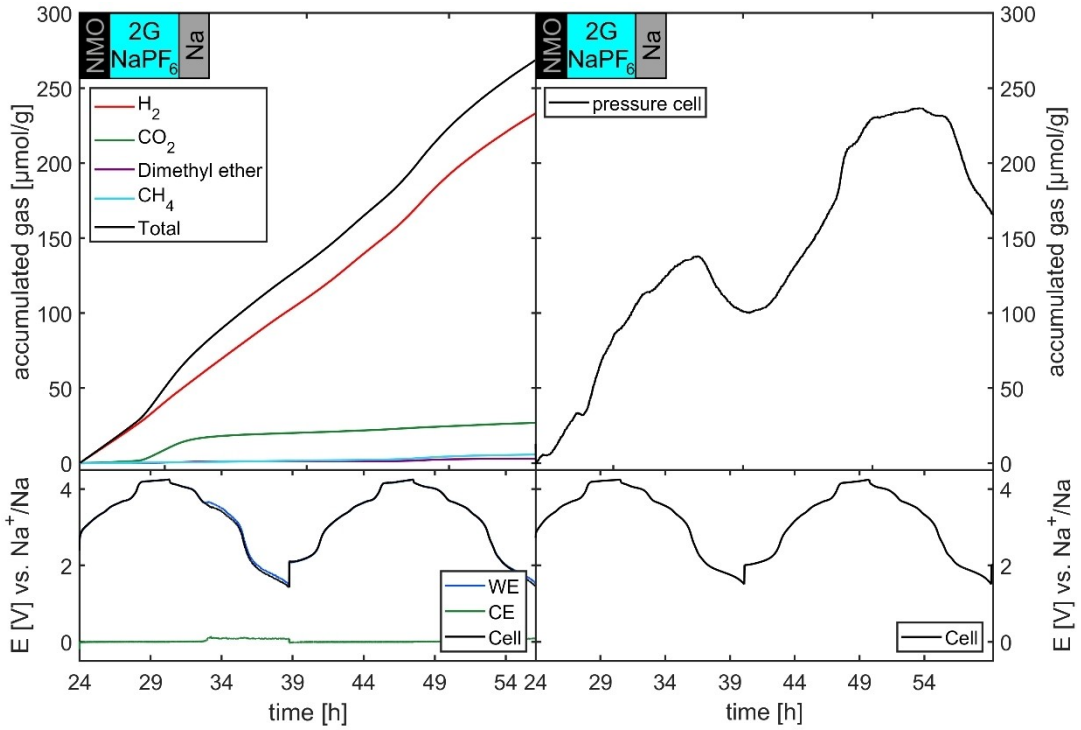

Figure 3. Accumulated gas formed over the first two cycles in 1 M $NaPF_6$ in 2G half-cells against sodium metal Integrated signals form DEMS cell (left) and calculated via ideal gas law form pressure cell at 25 °C (right). For the experiments the same electrodes and electrolyte volumes (relative to the geometric surface area of the working electrode) were used.

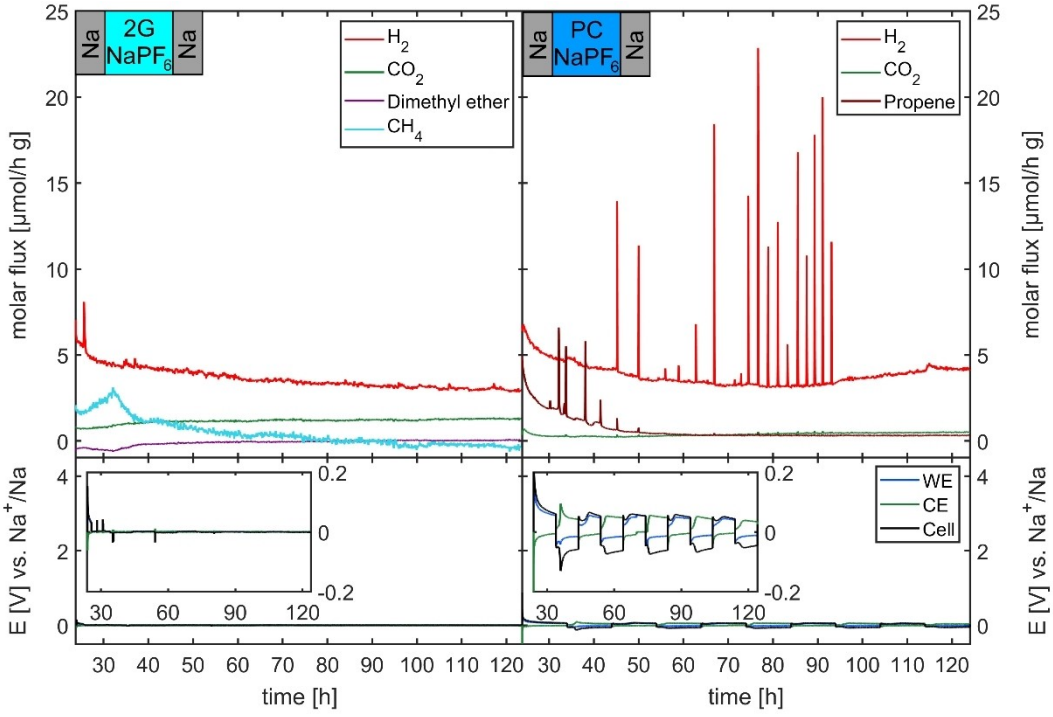

Figure 4. DEMS results for symmetric Na -Na cells for two different electrolyte solutions (1 M $NaPF_6$ in 2G and PC respectively). Plating and stripping is shown over 5 cycles at 0.11 mA/cm2 over 10 h intervals. To compare the gas release, the molar gas fluxes were normalized to the active material mass of the corresponding NaMNO cells, see further below. Spike-signals in the PC cell are from small gas-bubbles. The voltage profiles are given in the same scale as throughout this publication, the insets show magnifications, to highlight the higher polarization in the PC electrolyte.

Poor SEI formation of Na metal in carbonate electrolytes is a known issue in battery research.[17,65–68] Our results underline the general problem when comparing electrochemical measurements in a two-electrode configuration, particularly when using Li or Na as counter electrodes and different electrolyte formulations (ethers vs. carbonates). Unknown polarization effects at the counter electrodes can lead to different electrode potentials at the working electrodes. To avoid incorrect determination of the electrolyte or electrode stability, it is recommended to perform measurements in a three-electrode geometry.

3. Results

This section presents the DEMS results obtained for Na|Na symmetrical cells as well as Na|NaMNO half-cells. The electrode potentials of the working and counter electrodes were recorded using a Na metal reference electrode. All measurements were performed over 5 consecutive cycles. All cells were equilibrated for 24 hours prior to measurement. Since electrolyte decomposition typically occurs at high potentials, measurements were performed at two different cutoff potentials (3.80 V and 4.25 V vs. Na^+/Na). For all measurements, the gassing for electrolyte solutions of 1 M $NaPF_6$ in carbonate (PC) and ether (diglyme, 2G) are compared.

3.1. Na|Na Symmetrical Cells

Figure 4 shows the DEMS data for symmetric Na | Na cells with two different electrolytes over 5 plating/stripping cycles at 0.11 mA/cm^2 in intervals of 10 h. The current density is close to that used for the half-cells with NaMNO as the working electrode discussed below.

The lower figure shows that the electrode polarization is stronger in the case of PC, indicating, as expected, a more resistive SEI. Despite the subsequent plating and stripping, the gas release is continuous or decreases with time. This is consistent with findings in the literature that both carbonate[11] and diglyme[69] based electrolytes undergo continuous decomposition in contact with Na metal. H_2, CO_2 and propene are found for the PC electrolyte (as expected from literature[11]) while H_2, CO_2 and dimethyl ether are found for the 2G electrolyte.

The appearance of dimethyl ether (albeit in small amounts) is different from our previous study in where H_2, CO, CH_4 and ethylene were found for symmetrical cells with a 2G electrolyte.[17] This highlights the advantage of using the MCD algorithm and the full mass spectrum. Only the inclusion of dimethyl ether in the calibration matrix gave satisfactory results for the fitted spectra. The amount of dimethyl ether is very small, but can be observed more clearly in the half-cell experiments. The quality of the fit for both measurements is shown in Figure SI-3 in the Supporting Information. The detection of dimethyl ether is consistent with Qin *et al.* who suggested that this compound is a likely degradation product of 2G[13] and has been found in Li-O_2 batteries.[29]

The MCD algorithm also points out the difficulty of unambiguously detecting and quantifying CO by DEMS.[11,70] There is some literature reporting the formation of CO.[42,46,53,71,72] Here, the intensity of m/z = 28 is either taken directly, or is corrected for the fragments of other gases present, and the remaining signal is expected to be CO. Figure SI-8 in the Supporting Information shows the result when CO is included in the analysis. The CO signal shows strong drift and noise, and is additionally also strongly influenced by traces of N_2 as a background gas. The drift is caused by the indistinguishable assignment of the signal of m/z = 28 to either CO or N_2 by the MCD algorithm. Both gases show a strong intensity at m/z = 28 and only minor signals for other m/z values (12, 14, 16), which also overlap with other gases. While the calculation over the whole spectrum leads to a robust assignment of all signals to specific gases, small fluctuations and noise lead to very different calculated amounts for these two gases. Fortunately, with the exception of the nitrogen background, the inclusion of CO does not significantly affect the calculated amounts of the other gases formed. In other words, for the quantification of the other gases it does not matter whether CO is present or just an artifact. The strong drift of the CO signal is found for both cells with different solvents. This shows that, at least in our measurement setup, the amount of CO is not easy to determine even when using the MCD algorithm approach. CO is therefore not easy to distinguish from measurement artifacts and other methods such as IR spectroscopy should be used in parallel.[70]

Figure 4 also shows several sharp peaks for the PC electrolyte measurement. Similar features can be seen in some of the measurements throughout this study. Although these peaks look prominent, the peak area is very small and the related amount of gas is very small. We attribute these features to gas bubbles trapped on their way from the counter electrode through the separator and electrolyte to the gas stream. Figure SI-11 shows the data including the Ar background, which illustrates that the spikes occur simultaneously for all gases. While it would be a further improvement to the measurement to avoid these bubble formations, it shows how quickly the measurement system itself reacts to changes. An abrupt change in gas concentration, such as a popping bubble, results in a very sharp signal. This also means that signals with longer tails are not caused by slow gas transport, but rather the result of a longer gas evolution process.

3.2. Half-Cells with NaMNO ($Na_{0.67}Mn_{3/4}Ni_{1/4}O_2$) as the Working Electrode and High Cut-Off Potential of 4.25 V vs. Na^+/Na

The gases produced in sodium-symmetric cells can serve as a good indicator of the gases released from the counter electrode in half-cell experiments. In half-cells, the amount of gas released by the Na electrode alone should be approximately half of what is detected in the symmetrical cells. Additionally, as previously staated, gas release in the symmetric cells is rather continuous and does not vary when reversing plating/stripping. All changes

Research Article
doi.org/10.1002/batt.202400006
Chemistry Europe
European Chemical Societies Publishing

in gas release during cycling of the half-cells can be attributed to processes involving the NaMNO cathode. This can be evolution directly from the cathode or from crosstalk of side products between the cathode and anode.

The investigated P2 type NaMNO material is composed of spherical dense particles and exhibits solid solution behavior within the voltage range of 1.5–4.0 V, with a single P2 phase. At 4.2 V, it displays a voltage plateau and a two-phase reaction with an O2 phase. SEM images of the electrodes are presented in Figure 5. Previous research has demonstrated that the high voltage plateau is primarily responsible for the observed capacity fade of the material. This indicates that side reactions dominate at this state of charge, which is supported by the presented DEMS data. For a detailed description of the NaMNO material, refer to a recent publication,[34] that focuses on material synthesis and characterization.

The measurements presented in Figure 6 were conducted using 1 M $NaPF_6$ in 2G (left) and PC (right), within a voltage window of 1.5 V to 4.25 V vs. Na^+/Na reference.

H_2 as the main gas: H_2 is the major gas formed in both electrolytes, although the total amount is much higher in the case of PC. The formation of H_2 in DEMS measurements can be caused by a number of factors.[7,20] Trace water impurities are a common cause[59,73] but for several reasons we consider this unlikely to be the main source. All cell parts were carefully dried, and any remaining traces of water should have reacted with the Na metal prior to the measurements as the cells equilibrated over 24 hours. Trace water should also continuously react with Na metal, resulting in continuous H_2 evolution.[74] This is obviously not the case as the H_2 evolution changes over the cycles. Another indicator is the absence of signals for POF_3, which is a common product of the hydrolysis of PF_6^-. Taken together, these considerations strongly suggest that trace water is not the dominant source of H_2, but originates from electrolyte solvent degradation.[42]

For both electrolytes, the first cycle behaves differently from the following ones. Starting from the second cycle, a clear potential-dependent behavior is observed. In the case of 2G electrolyte, there is an initial increase in H_2 formation as the potential rises steeply during charging, followed by a second, stronger H_2 formation after reaching the high voltage plateau. The gas evolution increases up to the inflection point at the highest potential. During discharge, the H_2 signal decreases to a minimum at the lowest potential.

The two steps suggest that there are two distinct reactions leading to H_2 formation. The first peak (maximum at 3.3 V) is not visible in the first cycle and increases in subsequent cycles. This behavior indicates that the reactant for H_2 formation is not present at the beginning but forms during decomposition reactions at higher potentials. Therefore, the source of H_2 formation is related to processes in the previous cycle.

The first peak overlaps with the onset of a less pronounced step in the voltage profile. At this redox potential, the sodium content in the NaMNO structure is about 0.5, the conversion of Mn^{3+} to Mn^{4+} is complete, and Ni^{2+} begins to be oxidized to Ni^{3+}. This observed behavior is reproducible over several cycles and is found for different cells (see comparison Figure SI-7 in the Supporting Information). It seems plausible that the overlap is not a coincidence and reflects the properties of the electrode at this specific potential. For example, a certain catalytically active site is only present at potentials lower than 3.3 V during charging. This could be Mn^{3+}, which is known to be a good oxidizing catalyst in other fields due to its Jahn-Teller distortion[75–77] and the dissolution of Mn^{2+} from the disproportion of Mn^{3+}.[78] These processes could be the cause of the gas evolution at these potentials. On the other hand, one would also expect Ni^{3+} or Ni^{4+} to be active centers for dehydrogen-

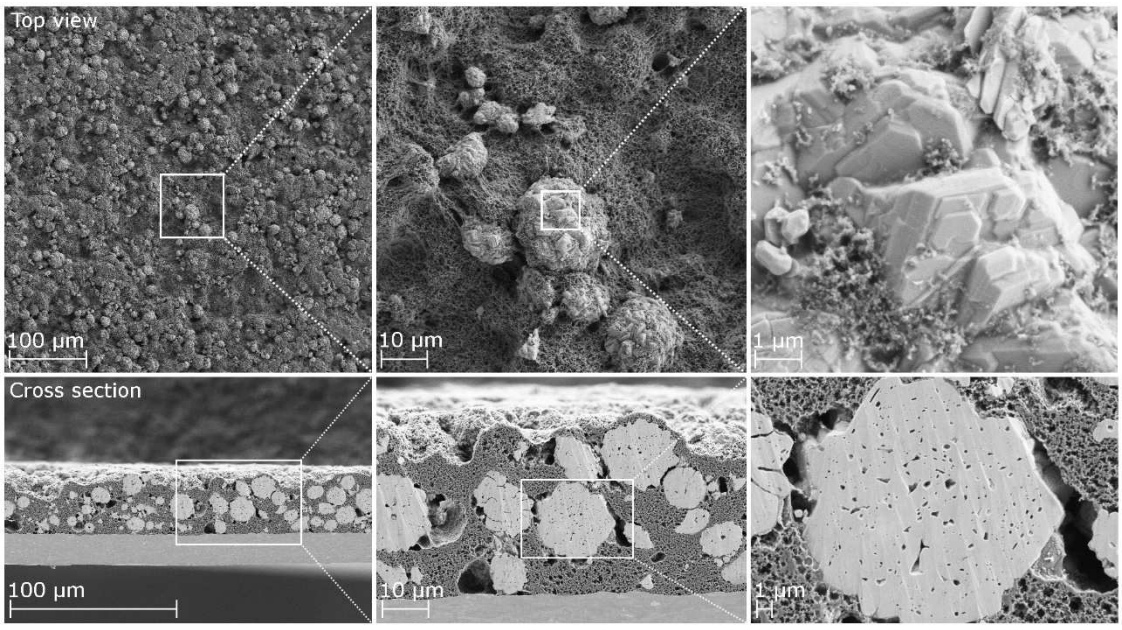

Figure 5. SEM images of the NaMNO electrode. Top-view (top) and cross section (bottom) with different magnification.

Research Article
doi.org/10.1002/batt.202400006
Chemistry Europe
European Chemical Societies Publishing

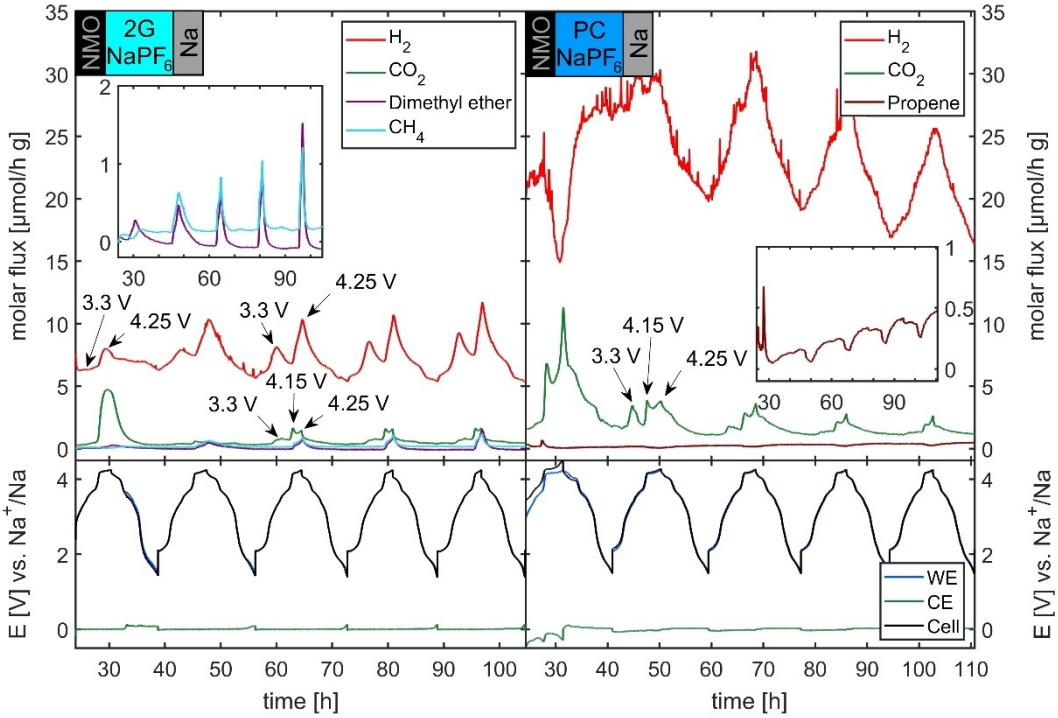

Figure 6. First five cycles of NaMNO cells with 1 M $NaPF_6$ electrolytes 2G (left) and PC (right) cycled in a voltage window of 1.5 to 4.25 V vs. Na^+/Na and current density of 20 mA g^{-1}. Na metal is used as counter and as reference electrode. Insets show magnification of the minor gas species.

ation and oxidation catalysts as well.[42,79,80] These should form at higher potentials and could also activate the surface oxygen to chemically react with the electrolyte.[71,81,82] Therefore, more active catalytic centers should form towards higher potentials, and gas evolution would be expected to further increase instead of showing a local maximum for a catalytic effect.

We propose that the H_2 at lower potentials is a diffusion limited reaction resulting from the further decomposition of species formed in the previous cycle. The reactants are depleted near the cathode, and therefore the gas evolution passes through the maximum at 3.3 V. Further evidence for this hypothesis is provided by the measurements with lower cut-off potential discussed below.

The minimum between the two H_2 peaks is at 3.9 V, in the middle of the steep slope towards the high voltage plateau. The H_2 evolution then increases again to its maximum at the upper cut-off potential. Throughout the discharge, the H_2 evolution decays slowly. This suggests that most of the oxidative electrolyte decomposition occurs during the high voltage plateau.

A better understanding of H_2 release can be obtained by considering the cross-talk between the two electrodes. Oxidation of the electrolyte or other electrode components, such as the conductive carbon results in protic species that can diffuse to the sodium metal counter electrode. The reduction of these protic species at the counter electrode then leads to the release of H_2, i.e. the formation of H_2 is due to cross-talk between the two electrodes. This was nicely demonstrated by Metzger *et al.* for Li-cells using a DEMS setup in which the cross-talk between the electrodes was eliminated by implementing a solid electrolyte membrane.[53] Similar results were reported by Michalak *et al.* using a LiMNO | graphite full-cell. They found an onset for CO_2 and H_2 evolution when Ni is completely converted to Ni^{3+} and Ni^{4+} starts to form, and that the H_2 evolution is mainly caused by the counter electrode.[83] Comparison of these findings with the present results indicates that the same decomposition processes occur in Li and Na layered oxides. The cross-talk mechanism is also consistent with the decrease in H_2 evolution during discharge, as the concentration of protic species decreases with decreasing potential.

Comparing the H_2 evolution for the 2G electrolyte with the PC electrolyte, one can qualitatively observe a similar cycle dependent behavior, although the two peaks are less defined in the case of PC. The first H_2 evolution peak appears as a shoulder at 3.5 V starting from the third cycle. This indicates that similar processes take place in both electrolytes, but a major difference is that the gas release for the PC electrolyte is about 4 times as much as for the 2G electrolyte. Theoretical calculations indicate that ketones and aldehydes are likely to be the first oxidative decomposition products of cyclic carbonates.[84] Since sodium metal can react as a strong base, the α-position to the carbonyl group should be acidic enough to be deprotonated under the release of hydrogen. It seems plausible that oxidation of 2G could also lead to the formation of aldehyde or ester species, but at lower rates. Such products, along with carbonate, formate, and acetate are known decomposition products in alkali metal air batteries.[85] The formation of these ketones and aldehydes, along with the overall stronger reaction with sodium metal, may explain the higher H_2 release for the PC electrolyte. On the other hand, supporting this hypothesis would require

the use of complementary analytical tools that also provide information on soluble and solid decomposition products.

Other gases: The second most commonly observed gas for both electrolytes is CO_2, which occurs mainly in the first cycle. The signal in the first cycle is also clearly different from the following ones, especially for 2G. The strong evolution in the first cycle can be attributed to the decomposition of carbonate impurities from the electrode material, as described for Li cells.[47,86] It is triggered by the presence of protic species, which can be formed by oxidation at elevated potentials. The CO_2 evolution for both electrolytes starts during the first cycle, at the beginning of the high voltage plateau. This suggests that protic decomposition products are formed at this point. Since the chemical reaction of the carbonates consumes protic species,[47] this could be another explanation for the H_2 evolution in the first cycle also being different and less intense compared to the following ones. The surface contamination with carbonates is discussed in detail in the publication on the synthesis of the here used material.[34]

During the subsequent cycles, the CO_2 evolution is significantly lower, and the distribution over the cycling profile is different. This indicates that most of the carbonate impurities are consumed during the first cycle. The CO_2 evolved in the consecutive cycles is produced through other reactions, such as the oxidation of the electrolyte or the conductive carbon.[71] Both electrolytes show the formation of three distinct CO_2 peaks. A smaller peak is observed at low potentials (3.3 V), while two overlapping peaks are observed at high potentials of 4.15 V and 4.25 V.

The two overlapping peaks are one at the beginning of the high voltage plateau and one at the upper cut-off voltage. This behavior can be seen for other materials as well.[15,54] An explanation for the first increase during the voltage step could be the cracking of the material, which creates a higher surface area,[87] while the second is more likely to be related to active lattice oxygen oxidizing the electrolyte. It has been shown that materials similar to the one presented here, $Na_{0.66}Ni_{0.33}Mn_{0.67}O_2$, undergo anionic oxygen redox[88] and show oxygen release at potentials above 4.2 V.[89] Alkali metal-rich layered oxides are known to undergo oxygen release at high potentials.[14–16] No evidence for oxygen release from the active material was found in the MS data. However, for some active materials, it is possible that reactive oxygen species react with the electrolyte or conductive additive to form CO_2, which is then detected by the MS.[71,74,90] This was shown with ^{18}O-labeled cathode materials of similar structure by House *et al.* While the lattice oxygen in P2-$Na_{0.67}Mg_{0.28}Mn_{0.72}O_2$ appeared stable, reactions involving lattice oxygen were found for the Li-stabilized layered oxide P2-$Na_{0.78}Li_{0.25}Mn_{0.75}O_2$.[14] Note that a slightly lower potential for CO_2 release has been reported for another layered oxide by X Ji *et al.*[91] However, a direct comparison should be made with caution because the composition of the electrode and electrolyte is slightly different and limited information is provided on the DEMS experiment and data analysis.

Figure SI-9 in the Supporting Information shows the fitting result including CO. As mentioned above, the correct incorporation of CO is challenging in general. While again some data drift is observed, the fit results nevertheless still indicate CO evolution in parallel with CO_2 formation at high potentials for both electrolytes.

CH_4 and dimethyl ether in the case of 2G evolve at potentials above 3.9 V, so they should be products of electrolyte oxidation at high potentials. The peaks of these gases increase from cycle to cycle, so intermediates must be formed first, or the surface reactivity of the electrode towards the decomposition increases over cycling. Another reason might be particle cracking, which leads to an increasing reactive surface area. This indicates poor stabilization of the electrode-electrolyte interface and suggests that film forming additives for the cathode active material (CEI formation) may be an important measure to increase the cycle life of SIBs.

In the case of PC, the propene signal shows a small peak at high potentials together with the first sharp increase in CO_2. The peak is absent in the following cycles, but the propene signal increases slightly over the cycles and shows minima together with the CO_2 release. Such a first peak of alkene formation is usually attributed to SEI formation at the anode, here Na metal.[11,74] Interestingly, no such cycle dependent behavior was observed in the symmetric Na|Na cell, but a more constant decay was observed at the beginning of the measurement. Propene is known to be the product of the ring-opening reaction of cyclic carbonates. This process is catalyzed in the presence of trace water and even stronger OH^- under battery operating conditions.[59] Since the peak occurs together with CO_2 evolution, which we attribute to decomposition of inorganic carbonates with protic species, we suggest that this initial propene peak is caused by ring-opening of PC under these protic conditions.

For another Ni/Mn-based layered oxide, it has been suggested that solvent molecules may enter the lattice when exceeding potentials of 4.0 V.[92] This would imply a larger contact area between the electrolyte and the active material, which could be the reason for higher gas evolution. Also, the P2–O2 phase transition occurs at about 4.15 V, which could also be a cause for higher reactivity.[93] Both suggestions would be consistent with our findings showing the highest gas evolution at these potentials. The longer high voltage plateau in the first cycle of the PC electrolyte is consistent with a greater amount of detected gas. The observed excess capacity is therefore likely the result of electrolyte decomposition.

3.3. Half-Cells with NaMNO ($Na_{0.67}Mn_{3/4}Ni_{1/4}O_2$) as Working Electrode and Low Cut-Off Potential of 3.80 V vs. Na^+/Na

It is known that lowering the upper cut-off potential can significantly improve the cycle life of NaMNO-type electrodes.[32,92,93] Experiments with the upper cut-off at 3.8 V vs. Na^+/Na confirm that the side reactions are mainly triggered at the high potentials. This potential is just at the onset to the high voltage plateau of the P2–O2 phase transition. The results of these measurements are shown in Figure 7. Lowering the cut-off potential obviously leads to a much lower overall gas release, even at lower voltages, only the H_2 signal during the

Research Article
doi.org/10.1002/batt.202400006
Chemistry Europe
European Chemical Societies Publishing

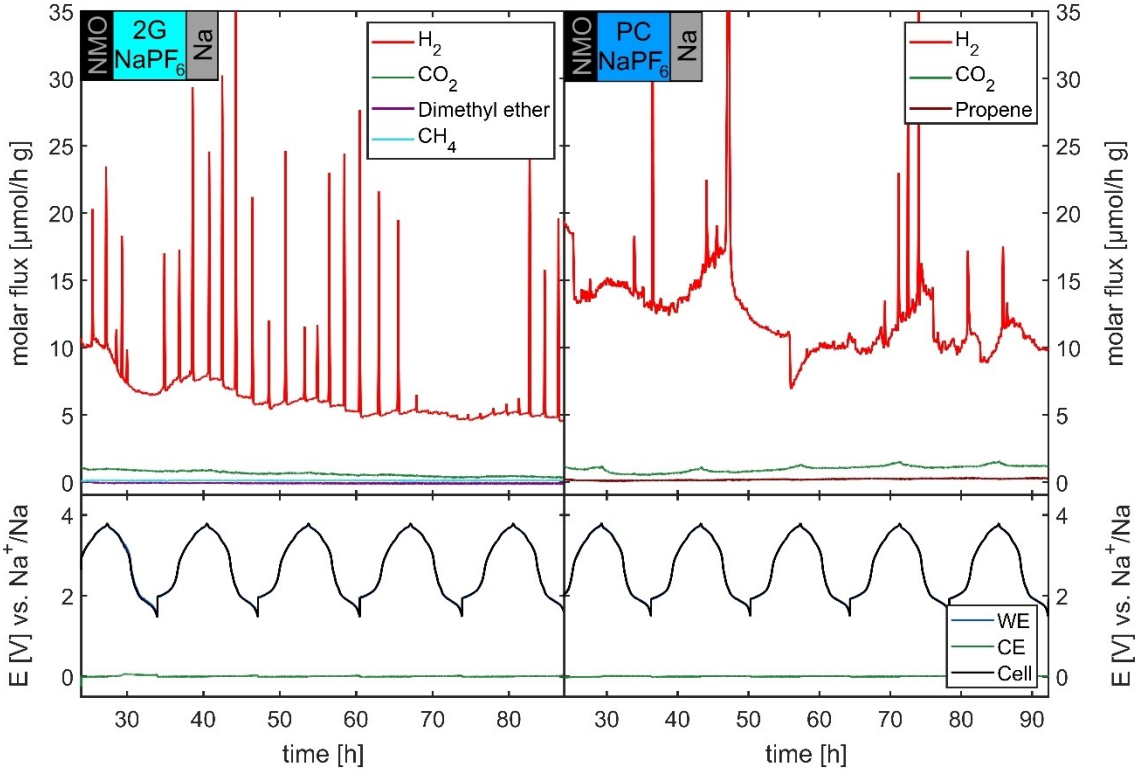

Figure 7. First five cycles of NaMNO cells with 1 M $NaPF_6$ electrolytes 2G (left) and PC (right) cycled in a voltage window of 1.5 to 3.8 V vs. Na^+/Na and current density of 20 mA g^{-1}. Counter and reference electrode from Na metal.

first cycle of the 2G cell is higher. However, this is within the range of deviation between similar cells. Figure SI-7 in the Supporting Information compares two identical 2G cells.

More significant than the reduction in total gas evolution is the reduction in cycle-dependent gas evolution. For the 2G-containing cell, the H_2 evolution shows only a small cycle-dependent increase above the expected baseline. For the PC containing cell, the overall H_2 evolution is about twice that of the Na|Na symmetric cell, but there is no consistent cycle-dependent evolution.

It can also be seen that reducing the cut-off potential to 3.8 V prevents the formation of CH_4, dimethyl ether and propene, respectively. A small and decaying CO_2 evolution is found in the 2G-containing cell. This might originate from a chemical reaction with the sodium metal or the slow decomposition of the carbonate impurities of the cathode, which now occurs over several cycles due to the lower cut-off potential. In the PC-containing cell, the CO_2 evolution is slightly higher compared to the Na|Na-symmetric cell, shows small peaks at potentials above 3.3 V, and the signal increases slightly over cycles.

Taking all the results together, most of the side reactions for the studied cell with NaMNO as the cathode active material are caused by oxidation reactions above 3.8 V. This includes the evolution of gases seen at lower potentials after the first cycle in the cells cycled to 4.25 V, proving that the reactants causing the gas evolution at low potentials around 3.3 V are mainly due to side products formed at higher potentials in the previous cycles. For $Na_{0.58}Ni_{1/3}Mn_{2/3}O_2$, Cai *et al.* identified 2.6–3.8 V as the stable voltage window and suggested that higher voltages cause side reactions due to the formation of O_2^{x-}-species.[94] This is in good agreement with what was found in the Mn-richer material studied here. Even if no O_2 release was found, the reactive oxygen species are likely to be the reason for the increased electrolyte oxidation at these potentials.

4. Conclusions

In this work we propose the use of a DEMS system with 3-electrode geometry combined with MCD analysis of the full MS spectra for the study of Na and Na-ion battery materials. The setup allows measurements for more than 200 hours before the cells are drying out. The MCD algorithm provides a robust data evaluation that allows to evaluate how well the full MS spectra can be fitted to a mixture of gases. This approach was validated using pressure monitoring during galvanostatic cycling.

The analysis was systematically applied to study the stability of NaMNO ($Na_{0.67}Mn_{3/4}Ni_{1/4}O_2$) as a positive electrode for Na-ion batteries in two different electrolytes based on diglyme and PC. The measurements were performed in half-cell geometry, as this is the most common cell configuration in research studies. The contribution of the Na counter electrodes to the gas release was studied using Na|Na symmetric cells and was found to be smaller in most cases compared to the reactions related to NaMNO. The study also emphasizes the relevance of using a

reference electrode, otherwise the stability of electrode materials may be overestimated.

For the NaMNO material, the major gas-forming side reactions are triggered at potentials exceeding 3.8 V vs. Na^+/Na. At potentials above 3.8 V, the known decomposition products H_2, CO_2 and propene for PC and H_2, CO_2 and methane for 2G are found. In addition, we show that dimethyl ether is a decomposition product of the 2G electrolyte in SIBs at these potentials. Gases formed at potentials around 3.3 V for cells cycled to 4.25 V can be suppressed by lowering the upper cut-off to 3.8 V. This suggests that the species reacting at these lower potentials were formed at higher potentials in the preceding cycle. H_2 formation is presumably caused by cross-talk of protic species. These species are formed at the NaMNO electrode during charging (oxidation) and then diffuse to the counter electrode where they are reduced. The measurements also indicate that Na_2CO_3 impurities from the synthesis of the NaMNO decompose when charged to 4.25 V, but several cycles are required when cycling to 3.8 V.

Interestingly, when looking at the overall gassing behavior, the 2G-based electrolyte seems to cause less side reactions compared to PC, even at high potentials. This is a rather surprising finding, as ethers are generally considered to have poorer oxidative stability. Nevertheless, additional measures are required for both electrolytes to allow higher charging voltages. The use of appropriate film forming additives (CEI formers),[95] coatings[96–98] or materials with composition gradients[99] are therefore, similar to LIBs, important strategies to further improve the performance of electrode materials for SIBs.[31] DEMS can certainly help to accelerate the search for stable cell chemistry and operating conditions.

Experimental Details

NaMNO Electrodes

The synthesis of the layered sodium manganese nickel oxide (P2-$Na_{0.67}Mn_{3/4}Ni_{1/4}O_2$) was carried out by hydroxide co-precipitation followed by mixing with sodium hydroxide and subsequent heat treatment in air. The co-precipitation was performed under vigorous stirring with aqueous solution of manganese nitrate (Carl Roth) and nickel nitrate (Carl Roth), sodium hydroxide (Carl Roth) and ammonia (Carl Roth) as continuous feeds into a continuously stirred tank reactor (CSTR, V = 1 l). The obtained dense, spherical hydroxide precursor ($Mn_{3/4}Ni_{1/4}(OH)_2$) was continuously filtered, dried, and mixed with an appropriate amount of sodium hydroxide (Carl Roth). Pre-calcination at 450 °C for 5 h in air was followed by calcination at 900 °C for 10 h in air. More details regarding the synthesis and characterization of the layered oxide can be found elsewhere.[34]

Cathode active material, PVDF binder (Solef P5130, Solvay) and conductive carbon (SuperP–Li, Timcal) in the respective weight ratio of 83.2 %, 8.3 %, 8.5 % are dispersed in appropriate amounts of n-methyl-2-pyrolidone (NMP, anhydrous, Sigma Aldrich). The resulting homogeneous slurry is casted on 20 μm aluminum foil using the doctor blade technique. After drying, the electrode sheets are calendered at 5 N/mm line pressure and 100 °C. Electrodes with a diameter of 38 mm are punched and dried overnight at 80 °C and dynamic vacuum in a Büchi glass oven.

Electrolytes

Solvents 2G (Sigma-Aldrich®, anhydrous, 99.5 % purity) and PC (Sigma-Aldrich®, 99.7 % purity) were stored for several days over a 1 : 1 mixture of 3 Å and 4 Å molecular sieves before use. $NaPF_6$ (Alfa Aeser®, 99 + % purity) was used as the electrolyte salt. The electrolytes were always freshly prepared just before the cells were assembled. The electrolytes thus prepared have a water content of < 10 ppm, which was determined by Karl Fischer titration.

DEMS Measurements

Cells were assembled in argon atmosphere. Before assembly, all cell parts were dried at 60 °C for at least 12 h. Whatman™ GF/A glass microfiber filters were used as separators, those were dried at 110 °C under vacuum overnight. A piece of sodium metal serves as reference electrode. For the counter electrode, sodium metal was roll-pressed to a flat foil using a standard kitchen pasta machine. The working electrode was placed in the top of the cell towards the current collector with the gas flow field. 1.6 mL of 1 M electrolyte was used in each cell. A resting time of 24 h was applied before the cycling started. Cycling for all cells was performed at 20 $mA\,g^{-1}$ in reference to the NaMNO active material. For the symmetrical Na|Na cells, the same current was used as for the PC cell with 4.25 V cut-off. This current is in the same range as all cells shown in this paper. The duration of a half-cycle was set to 10 h, which is just a little longer than expected for the NaMNO at 20 $mA\,g^{-1}$.

Pressure Cell

Pressure measurements were performed with an El-Cell® PAT-Cell-Press. All parameters were set to be the same as the compared DEMS measurements. The same materials were used. With respect to the geometric electrode area, which was 1.13 cm^2, 160 μL of electrolyte was used. The measurements were conducted in a climatic chamber at 25 °C. Note that the PAT-Cell-Press allows 3-electrode measurements, but this requires special ring reference electrodes, which were not available for Na during the course of the study.

Acknowledgements

The project received funding from the Bundesministerium für Bildung und Forschung (BMBF) over the projects TRANSITION (03XP0186B), TRANSITION Transfer (03XP0533C) and DIALYSORB (03XP0410C) and from the European Research Council (ERC) under the European Union's Horizon 2020 research and innovation programme (grant agreement No. [864698], SEED). The authors thank Alexander Schiele and Balasz Berkes for their kind introduction to their DEMS system at BELLA at KIT and to Erik Berg from Uppsala University for a productive discussion about DEMS and the handling of data. Open Access funding enabled and organized by Projekt DEAL.

Conflict of Interests

The authors declare no conflict of interest.

Data Availability Statement

The data that support the findings of this study are available from the corresponding author upon reasonable request.

Keywords: OEMS · sodium ion batteries · sodium manganese nickel oxide (NaMNO) · multiple concentration determination (MCD)

[1] J. Xiao, *et al., Mater. Chem. Front.* **2021**, *5*, 3735–3764; 10.1039/D1QM00179E.
[2] H. S. Hirsh, *et al., Energy Mater.* **2020**, *10*, 2001274; 10.1002/aenm.202001274.
[3] C. Delmas, *Adv. Energy Mater.* **2018**, *8*, 1703137; 10.1002/aenm.201703137.
[4] S. L. Dreyer, A. Kondrakov, J. Janek, T. Brezesinski, *J. Mater. Res.* **2022**, *37*, 3146–3168; 10.1557/s43578-022-00586-2.
[5] P. K. Nayak, L. Yang, W. Brehm, P. Adelhelm, *Angew. Chem. Int. Ed.* **2018**, *57*, 102–120; 10.1002/anie.201703772.
[6] J.-M. Tarascon, *Joule* **2020**, *4*, 1616–1620; 10.1016/j.joule.2020.06.003.
[7] B. Rowden, N. Garcia-Araez, *Energy Rep.* **2020**, *6*, 10–18; 10.1016/j.egyr.2020.02.022.
[8] O. Wolter, J. Heitbaum, *Ber. Bunsenges. Phys. Chem.* **1984**, *88*, 2–6; 10.1002/bbpc.19840880103.
[9] N. Schlüter, P. Novák, D. Schröder, *Adv. Energy Mater.* **2022**, *12*, 2200708; 10.1002/aenm.202200708.
[10] C. Delmas, D. Carlier, M. Guignard, *Adv. Energy Mater.* **2021**, *11*, 2001201; 10.1002/aenm.202001201.
[11] L. Zhang, C. Tsolakidou, S. Mariyappan, J.-M. Tarascon, S. Trabesinger, *Energy Storage Mater.* **2021**, *4*, 1616; 10.1016/j.ensm.2021.07.005.
[12] M. Goktas, *et al., Adv. Energy Mater.* **2018**, *8*, 1702724; 10.1002/aenm.201702724.
[13] B. Qin, *et al., ACS Appl. Mater. Interfaces* **2020**, *12*, 3697–3708; 10.1021/acsami.9b20616.
[14] R. A. House, *et al., Mater.* **2019**, *31*, 3293–3300; 10.1021/acs.chemmater.9b00227.
[15] U. Maitra, *et al., Nat. Chem.* **2018**, *10*, 288–295; 10.1038/nchem.2923.
[16] Q. Wang, *et al., Nat. Mater.* **2021**, *20*, 353–361; 10.1038/s41563-020-00870-8.
[17] M. Goktas, *et al., ACS Appl. Mater. Interfaces* **2019**, *11*, 32844–32855; 10.1021/acsami.9b06760.
[18] W. Liu, *et al., ACS Appl. Mater. Interfaces* **2019**, *11*, 23207–23212; 10.1021/acsami.9b05005.
[19] Y. Ma, *et al., Adv. Mater.* **2021**, *33*, e2101342; 10.1002/adma.202101342.
[20] O. C. Harris, S. E. Lee, C. Lees, M. Tang, *J. Phys. Energy* **2020**, *2*, 32002; 10.1088/2515-7655/ab8b68.
[21] S. Kim, *et al., Adv. Energy Mater.* **2023**, *13*, 2301983; 10.1002/aenm.202301983.
[22] J. Zhang, *et al., Adv. Energy Mater.* **2018**, *8*, 1801361; 10.1002/aenm.201801361.
[23] T. Palaniselvam, *et al., Adv. Funct. Mater.* **2019**, *29*, 1900790; 10.1002/adfm.201900790.
[24] J. Huang, *et al., Energy Environ. Sci.* **2019**, *12*, 1550–1557; 10.1039/C8EE03632B.
[25] B. Zhang, *et al., Adv. Mater.* **2016**, *28*, 9824–9830; 10.1002/adma.201603212.
[26] P. Adelhelm, *et al., Beilstein J. Nanotechnol.* **2015**, *6*, 1016–1055; 10.3762/bjnano.6.105.
[27] Y. Li, *et al., Nat. Energy* **2022**, *7*, 511–519; 10.1038/s41560-022-01033-6.
[28] Z. Wang, *et al., Small* **2020**, *16*, e2003268; 10.1002/smll.202003268.
[29] N. Tsiouvaras, S. Meini, I. Buchberger, H. A. Gasteiger, *J. Electrochem. Soc.* **2013**, *160*, A471–A477; 10.1149/2.042303jes.
[30] S. Meini, *et al., Phys. Chem. Chem. Phys.* **2013**, *15*, 11478–11493; 10.1039/C3CP51112J.
[31] J. Song, B. Xiao, Y. Lin, K. Xu, X. Li, *Adv. Energy Mater.* **2018**, *8*, 1703082; 10.1002/aenm.201703082.
[32] A. Gutierrez, *et al., J. Phys. Chem. C* **2018**, *122*, 23251–23260; 10.1021/acs.jpcc.8b05537.
[33] P. Manikandan, D. Ramasubramonian, M. M. Shaijumon, *Electrochim. Acta* **2016**, *206*, 199–206; 10.1016/j.electacta.2016.04.138.
[34] L. F. Pfeiffer, *et al., Front. Energy Res.* **2022**, *10*, 910842; 10.3389/fenrg.2022.910842.
[35] W. Zuo, *et al., Acc. Chem. Res.* **2023**, *56*, 284–296; 10.1021/acs.accounts.2c00690.
[36] L. Chang, *et al., J. Energy Storage* **2023**, *73*, 109025; 10.1016/j.est.2023.109025.
[37] S. Wang, C. Sun, N. Wang, Q. Zhang, *J. Mater. Chem. A* **2019**, *7*, 10138–10158; 10.1039/C8TA12441H.
[38] Q. Shen, *et al., Adv. Funct. Mater.* **2021**, *31*, 2106923; 10.1002/adfm.202106923.
[39] L. Yang, *et al., Adv. Funct. Mater.* **2021**, *31*, 2102939; 10.1002/adfm.202102939.
[40] Y. Li, *et al., Adv. Mater.* **2024**, e2309842; 10.1002/adma.202309842.
[41] Q. Shen, *et al., Adv. Energy Mater.* **2023**, *13*, 2203216; 10.1002/aenm.202203216.
[42] Z. Jusys, M. Binder, J. Schnaidt, R. J. Behm, *Electrochim. Acta* **2019**, *314*, 188–201; 10.1016/j.electacta.2019.05.076.
[43] H. Hahn, R. Wagner, F. Schappacher, M. Winter, S. Nowak, *J. Electroanal. Chem.* **2016**, *772*, 52–57; 10.1016/j.jelechem.2016.04.023.
[44] M. Holzapfel, A. Würsig, W. Scheifele, J. Vetter, P. Novák, *J. Power Sources* **2007**, *174*, 1156–1160; 10.1016/j.jpowsour.2007.06.182.
[45] B. B. Berkes, *et al., Anal. Chem.* **2015**, *87*, 5878–5883; 10.1021/acs.analchem.5b01237.
[46] M. Metzger, C. Marino, J. Sicklinger, D. Haering, H. A. Gasteiger, *J. Electrochem. Soc.* **2015**, *162*, A1123–A1134; 10.1149/2.0951506jes.
[47] A. T. S. Freiberg, J. Sicklinger, S. Solchenbach, H. A. Gasteiger, *Electrochim. Acta* **2020**, *346*, 136271; 10.1016/j.electacta.2020.136271.
[48] F. Linsenmann, D. Pritzl, H. A. Gasteiger, *J. Electrochem. Soc.* **2019**, *166*, A3668–A3674; 10.1149/2.0741915jes.
[49] A. Bhide, J. Hofmann, A. K. Dürr, J. Janek, P. Adelhelm, *Phys. Chem. Chem. Phys.* **2014**, *16*, 1987–1998; 10.1039/c3cp53077a.
[50] H. Wang, *et al., Anal. Chem.* **2014**, *86*, 6197–6201; 10.1021/ac403317d.
[51] P. Novák, *et al., J. Power Sources* **2000**, *90*, 52–58; 10.1016/S0378-7753(00)00447-X.
[52] A. A. Abd-El-Latif, *et al., TrAC Trends Anal. Chem.* **2015**, *70*, 4–13; 10.1016/j.trac.2015.01.015.
[53] M. Metzger, B. Strehle, S. Solchenbach, H. A. Gasteiger, *J. Electrochem. Soc.* **2016**, *163*, A798–A809; 10.1149/2.1151605jes.
[54] A. Guéguen, *et al., J. Electrochem. Soc.* **2016**, *163*, A1095–A1100; 10.1149/2.0981606jes.
[55] T. Teufl, *et al., J. Electrochem. Soc.* **2020** *167*, 110505; 10.1149/1945-7111/ab9e7f.
[56] K. N. Shitaw, *et al., Adv. Funct. Mater.* **2021**, *31*, 2006951; 10.1002/adfm.202006951.
[57] E. Castel, E. J. Berg, M. El Kazzi, P. Novák, C. Villevieille, *Chem. Mater.* **2014**, *26*, 5051–5057; 10.1021/cm502201z.
[58] U. Mattinen, M. Klett, G. Lindbergh, R. Wreland Lindström, *J. Power Sources* **2020**, *477*, 228968; 10.1016/j.jpowsour.2020.228968.
[59] M. Metzger, B. Strehle, S. Solchenbach, H. A. Gasteiger, *J. Electrochem. Soc.* **2016**, *163*, A1219–A1225; 10.1149/2.0411607jes.
[60] J. F. O'Hanlon, *A user's guide to vacuum technology / John F. O'Hanlon.* 3rd ed. (Hoboken, NJ : Wiley-Interscience, Hoboken, NJ, 2003).
[61] He, M. Elucidating interface reactions in Li-ion batteries and supercapacitors by in situ gas analysis. ETH Zurich, 2016.
[62] R. Lundström, E. J. Berg, *J. Power Sources* **2021**, *485*, 229347; 10.1016/j.jpowsour.2020.229347.
[63] P. Hartmann, *et al., Phys. Chem. Chem. Phys.* **2013**, *15*, 11661–11672; 10.1039/c3cp50930c.
[64] S. Gourang Patnaik, I. Escher, G. A. Ferrero, P. Adelhelm, *Batteries & Supercaps* **2022**, *5*, e202200043; 10.1002/batt.202200043.
[65] M. Dahbi, *et al., ChemElectroChem* **2016**, *3*, 1856–1867; 10.1002/celc.201600365.
[66] D. I. Iermakova, R. Dugas, M. R. Palacín, A. Ponrouch, *J. Electrochem. Soc.* **2015**, *162*, A7060–A7066; 10.1149/2.0091513jes.
[67] G. G. Eshetu, *et al., Adv. Energy Mater.* **2020**, *10*, 2000093; 10.1002/aenm.202000093.
[68] K. Pfeifer, *et al., ChemSusChem* **2019**, *12*, 3312–3319; 10.1002/cssc.201901056.
[69] K. Westman, *et al., ACS Appl. Energ. Mater.* **2018**, *1*, 2671–2680; 10.1021/acsaem.8b00360.
[70] B. B. Berkes, A. Jozwiuk, H. Sommer, T. Brezesinski, J. Janek, *Electrochem. Commun.* **2015**, *60*, 64–69; 10.1016/j.elecom.2015.08.002.
[71] R. Jung, M. Metzger, F. Maglia, C. Stinner, H. A. Gasteiger, *J. Phys. Chem. Lett.* **2017**, *8*, 4820–4825; 10.1021/acs.jpclett.7b01927.

[72] A. T. S. Freiberg, M. K. Roos, J. Wandt, R. de Vivie-Riedle, H. A. Gasteiger, *J. Phys. Chem. A* **2018**, *122*, 8828–8839; 10.1021/acs.jpca.8b08079.
[73] R. Bernhard, M. Metzger, H. A. Gasteiger, *J. Electrochem. Soc.* **2015**, *162*, A1984–A1989; 10.1149/2.0191510jes.
[74] R. Jung, M. Metzger, F. Maglia, C. Stinner, H. A. Gasteiger, *J. Electrochem. Soc.* **2017**, *164*, A1361–A1377; 10.1149/2.0021707jes.
[75] A. Ramírez, *et al., J. Phys. Chem. C* **2014**, *118*, 14073–14081; 10.1021/jp500939d.
[76] N. Sergienko, J. Radjenovic, *Appl. Catal. B* **2020**, *267*, 118608; 10.1016/j.apcatb.2020.118608.
[77] A. Indra, P. W. Menezes, M. Driess, *ChemSusChem* **2015**, *8*, 776–785; 10.1002/cssc.201402812.
[78] J.-H. Hong, M.-Y. Wang, Y.-Y. Du, L. Deng, G. He, *J. Mater. Sci. Mater. Electron.* **2019**, *30*, 4006–4013; 10.1007/s10854-019-00687-5.
[79] Z. Zhang, *et al., Chin. J. Catal.* **2018**, *39*, 1228–1239; 10.1016/S1872-2067(18)63055-4.
[80] M. T. Bender, Y. C. Lam, S. Hammes-Schiffer, K.-S. Choi, *J. Am. Chem. Soc.* **2020**, *142*, 21538–21547; 10.1021/jacs.0c10924.
[81] Y. Yu, *et al., J. Phys. Chem. C* **2018**, *122*, 27368–27382; 10.1021/acs.jpcc.8b07848.
[82] T. M. Østergaard, *et al., J. Phys. Chem. C* **2018**, *122*, 10442–10449; 10.1021/acs.jpcc.8b01713.
[83] B. Michalak, *et al., Anal. Chem.* **2016**, *88*, 2877–2883; 10.1021/acs.analchem.5b04696.
[84] E. G. Leggesse, R. T. Lin, T.-F. Teng, C.-L. Chen, J.-C. Jiang, *J. Phys. Chem. A* **2013**, *117*, 7959–7969; 10.1021/jp403436u.
[85] R. Black, *et al., ChemSusChem* **2016**, *9*, 1795–1803; 10.1002/cssc.201600034.
[86] Y. Bi, *et al., RSC Adv.* **2016**, *6*, 19233–19237; 10.1039/C6RA00648E.
[87] K. Wang, P. Yan, M. Sui, *Nano Energy* **2018**, *54*, 148–155; 10.1016/j.nanoen.2018.09.073.
[88] K. Dai, *et al., Nano Energy* **2020**, *74*, 104831; 10.1016/j.nanoen.2020.104831.
[89] Y. Zhang, *et al., ACS Cent. Sci.* **2020**, *6*, 232–240; 10.1021/acscentsci.9b01166.
[90] J. Wandt, A. T. S. Freiberg, A. Ogrodnik, H. A. Gasteiger, *Mater. Today* **2018**, *21*, 825–833; 10.1016/j.mattod.2018.03.037.
[91] H. Ji, *et al., Adv. Funct. Mater.* **2022**, *32*, 10.1002/adfm.202109319.
[92] Q. Liu, *et al., J. Mater. Chem. A* **2019**, *7*, 9215–9221; 10.1039/C8TA11927A.
[93] D. H. Lee, J. Xu, Y. S. Meng, *Phys. Chem. Chem. Phys.* **2013**, *15*, 3304–3312; 10.1039/c2cp44467d.
[94] X. Cai, *et al., J. Alloys Compd.* **2020**, *820*, 153093; 10.1016/j.jallcom.2019.153093.
[95] R. Mogensen, S. Colbin, R. Younesi, *Batteries & Supercaps* **2021**, *4*, 791–814; 10.1002/batt.202000252.
[96] J. Alvarado, *et al., ACS Appl. Mater. Interfaces* **2017**, *9*, 26518–26530; 10.1021/acsami.7b05326.
[97] J. H. Jo, *et al., Adv. Funct. Mater.* **2018**, *28*, 1705968; 10.1002/adfm.201705968.
[98] Y. Liu, *et al., Nano Energy* **2016**, *27*, 27–34; 10.1016/j.nanoen.2016.06.026.
[99] Y. Li, *et al., Nano Energy* **2016**, *19*, 522–531; 10.1016/j.nanoen.2015.07.019.

Manuscript received: January 5, 2024
Revised manuscript received: March 18, 2024
Version of record online: June 14, 2024